

## Chapter 4

# Quasi-dynamic versus fully-dynamic simulations of earthquakes sequences on heterogeneous faults with and without enhanced coseismic weakening

*Marion Thomas, Nadia Lapusta, Hiroyuki Noda, and Jean-Philippe Avouac*

### Abstract

Theoretical fault models and computer simulations of fault slip can reveal the role and relative importance of different factors on the manner in which slip accumulates on faults. Such factors include various forms and parameters of friction laws, pore pressure evolution, and fault non-planarity. To study long deformation histories, most simulation methods do not incorporate full inertial effects during simulated fast slip. In quasi-static methods, a series of static problems is solved, with the loading advanced in time. However, such methods cannot simulate fast slip during seismic events, and earthquakes have to be added to such simulations in a kinematic fashion. That is why so-called quasi-dynamic methods have become increasingly popular, which approximately account for inertial effects (and hence seismic radiation) during simulated earthquakes through a radiation damping term. Such methods allow to continue simulations through the seismic phase, without having to pay significant additional memory and computational costs associated with modeling true wave-mediated effects.

In this study, we compare the results of quasi-dynamic simulations and fully-dynamic ones, in which all wave effects are accounted for during simulated earthquakes. We consider the long-term fault

behavior in two problems: (i) interaction of two velocity-weakening regions separated by a small velocity-strengthening patch and (ii) segments with additional pronounced rate-weakening during seismic slip. We find that, in the absence of additional seismic weakening, the two methods generally result in the same qualitative behavior, with similar slip patterns, although there are quantitative differences. In fact, in quasi-dynamic simulation, resulting seismic events tend to have much slower slip velocity and rupture speeds which may modify significantly the resulting seismic events and hence the long-term fault behavior. In simulations with additional coseismic rate weakening, the two methods produce qualitatively different long-term results with different slip patterns. Fully-dynamic solution generates pulse-like events, while quasi-dynamic formulation turns earthquakes to be more crack-like. Moreover, we observe that the levels of shear stress on the fault is significant different in both cases. In fully-dynamic simulations seismic events are able to nucleate and to propagate through the fault at a much lower level of shear stress than for quasi-dynamic ones.

## 4.1 Introduction

The expanding stream of seismic and geodetic observations on major faults provide increasingly better insight into the variability of fault slip behaviors over a wide range of temporal and spatial scales, from quasi-instant coseismic slip that generates seismic waves to slower interseismic and postseismic slips of the order of few cm/yr that can include transient events (few days to a few months) with sliding rates 10 to 100 times larger than the plate rate (e.g, *Kanamori and Hauksson, 1992; Kawasaki et al., 1995; Linde et al., 1996; Heki et al., 1997; Freymueller et al., 2000; Wallace et al., 2004; Cross and Freymueller, 2007; Fournier and Freymueller, 2007; Chlieh et al., 2008; Perfettini et al., 2010; Loveless and Meade, 2011; Miyazaki et al., 2011; Evans et al., 2012; Burgmann et al., 2000; Titus et al., 2006; Murray et al., 2001; Jolivet et al., 2012; Kaneko et al., 2013*). These observations suggest a complex pattern of slip in the 0-50 km seismogenic depth range, with the fault interface likely consisting of interfingered patches that either creep at a low rate, without seismic radiation, or remain locked during the interseismic period and rupture seismically. It has been observed that this segmentation have a strong influence on the seismic rupture patterns (*Burgmann et al., 2005; Hetland and Hager, 2006; Chlieh et al., 2008; Kaneko et al., 2010; Perfettini et al., 2010; Chlieh et al., 2011; Loveless and Meade, 2011*): locked segments may rupture independently or together with neighboring patches, producing irregular earthquakes of different sizes. This complex behavior arises from the interaction of stress transfers, levels of prestress, and fault friction properties (*Rundle et al., 1984; Cochard and Madariaga, 1996; Ariyoshi et al., 2009; Kaneko et al., 2010*).

Understanding the physics and mechanics of the fault behavior is an important issue in seismotectonics, since the seismic potential of any fault depends primarily on the partitioning between seismic and aseismic slip. Theoretical fault models and computer simulations of fault slip can reveal

the role and relative importance of different factors on the manner in which slip accumulates on faults and can provide physical basis for understanding the entire earthquake sequence.

To study the factors controlling the fault behavior, it is essential to incorporate all the stages of the fault deformation into a single physics-based model. Simulating the behavior of the model requires algorithms that are able to treat all aspects of the observed fault slip, from long-duration deformation histories, with continuous aseismic creep throughout the loading period, to gradual nucleation of earthquakes, followed by dynamic propagation of ruptures and rapid post-dynamic deformation after such events. Indeed, prestress inherited from aseismic slip history and prior seismic events would determine where earthquakes would nucleate and how far the rupture would propagate. However, realistic simulations that account for full inertial (wave) effects during seismic events as well as long-term deformation history are challenging because of the variety of temporal and spatial scales involved. That is why many modeling efforts of long fault slip histories simplify the representation of the dynamic events (e.g. *Shibazaki and Matsuura, 1992; Cochard and Madariaga, 1996; Kato, 2004; Duan and Oglesby, 2005; Liu and Rice, 2005; Hillers et al., 2006; Ziv and Cochard, 2006*). A common approximation is the quasi-dynamic (QD) model (*Rice, 1993; Ben-Zion and Rice, 1995; Rice and Ben-Zion, 1996; Hori et al., 2004; Kato, 2004; Hillers et al., 2006; Ziv and Cochard, 2006*) in which the wave-mediated stress transfers are ignored. In the QD simulations, inertial effects during simulated earthquakes are approximately accounted for through a radiation damping term. This method allows computing the long-term histories of fault slip, including the seismic phase, without having to pay significant additional memory and computational costs associated with modeling true wave-mediated effects. However, the question arises as to how the results of simulations are influenced by ignoring this part of the dynamic response (*Lapusta et al., 2000; Lapusta and Liu, 2009*).

Here, we explore our hypothesis that the QD simulations can only be qualitatively useful in situations where the wave-mediated stress transfers do not produce qualitatively important features that define the model response. To that end, we study two conceptually different physical models. In the first one, only the standard rate-and-state friction laws (Dieterich, Ruina) are used, as in *Lapusta et al. (2000); Lapusta and Liu (2009)*. In the other one, enhanced dynamic weakening is added motivated by flash heating (Rice 2006), which have been shown to result in self-healing pulses on low-prestressed faults (*Zheng and Rice, 1998; Noda et al., 2009*). The self-healing mode is generated through appropriate stress transfers by dynamic waves, and hence the QD approach should not be able to capture it. We indeed find that the QD and fully dynamic (FD) simulations produce dramatically different results in the model with the enhanced weakening. Similarly dramatic differences between the QD and FD approach are expected in other situations where wave-mediated effects play a significant role, such as in the models with transitions to supershear speeds (e.g., *Andrews, 1976; Xia et al., 2004; Liu and Lapusta, 2008*). We also consider how the QD and FD

simulations compare with respect to rupture interaction with a potential local barrier in the form of a fault region with velocity-strengthening friction, following the study of *Kaneko et al.* (2010).

Our methodology is described in section 4.2, with a particular emphasis on the differences between the FD and QD approaches. Section 4.3 confronts the FD and QD simulations of earthquake sequences with the standard rate-and-state laws. In section 4.4, we consider how fault response compares when enhanced coseismic weakening is added in the FD and QD cases. The reasons for the dramatic differences between FD and QD simulations with enhanced weakening are discussed in section 4.5. In section 4.6 we explore the ability of the earthquake rupture to propagate over faults with heterogeneous properties for the two different friction laws models used in this paper, with or without full wave-mediated effects. Our findings are summarized in section 4.7.

## 4.2 Methodology

### 4.2.1 Fully dynamic vs quasi dynamic formulation

We consider a 2-D antiplane (Mode III) model, with 1D fault embedded in a 2D uniform, isotropic, elastic medium. Earthquakes occur spontaneously on the fault subject to slow tectonic loading. The model has been fully described by *Lapusta et al.* (2000). Nevertheless, in order to understand the difference between QD and FD formulation, it is useful to recall the underlying elastodynamic equations. We assume purely dip-slip motion on a fault which coincides with the  $x - z$  plane of a Cartesian coordinate system  $xyz$ . The only non-zero displacement  $u_x(y, z, t)$  is along-strike (parallel to the  $x$  direction). Then the time-dependent relative slip  $\delta(z, t)$  corresponds to the displacement discontinuity  $\delta(z, t) = u_x(0^+, z, t) - u_x(0^-, z, t)$ . The relevant shear stress on the fault plane  $\tau(z, t) = \sigma_{xy}(0, z, t)$  is expressed as the sum of a loading term  $\tau^0(z, t)$ , i.e. the stress that would act in absence of any displacement continuity on the fault plane  $y = 0$ , and some additional terms related to slip  $\delta(z, t)$  (*Perrin et al.*, 1995; *Cocharad and Madariaga*, 1996; *Lapusta et al.*, 2000):

$$\tau(z, t) = \tau^0(z, t) + f(z, t) - \frac{\mu}{2c_s} V(z, t), \quad (4.1)$$

where  $\mu$  is the shear modulus,  $c$  is the shear wave speed and  $V(z, t) = \partial\delta(z, t)/\partial t$  is the slip rate. In equation (4.1), the functional  $f(z, t)$  incorporates most of the elastodynamic response and represents the stress transfer along the fault through waves. It is a linear functional of prior slip  $\delta'(z', t')$  over the causality cone, that expresses the stress transfer due to a rupture. The third term,  $\frac{\mu}{2c} V(z, t)$  represents the radiation damping term (energy radiated by waves in the medium) (*Rice*, 1993). Explicit extraction of that term from the functional  $f(z, t)$  avoids singularities of the convolution integrals (*Cocharad and Madariaga*, 1996).

The difference between FD and QD models lies in the expression of the stress-transfer functional

$f(z, t)$ , which involves a double convolution integral in space and time. In the spectral domain,  $f(z, t)$  is related to  $\delta(z, t)$  by a single convolution integral in time when slip and the functional are represented as truncated Fourier series in space (*Perrin et al.*, 1995). This is very advantageous, as convolution integrals are the most computationally demanding part of the elastodynamic analysis. Let us write:

$$\delta(z, t) = \sum_{n=-N/2}^{N/2} D_n(t) e^{ik_n z}, \quad (4.2)$$

$$f(z, t) = \sum_{n=-N/2}^{N/2} F_n(t) e^{ik_n z}, \quad k_n = \frac{2\pi n}{\lambda}, \quad (4.3)$$

where  $\lambda$  is the length of the fault domain, replicated periodically and discretized into  $N$  (even) elements. The period  $\lambda$  has to be larger than the domain over which the seismic rupture takes place, to avoid influence of waves arriving from periodic replicates of the rupture. To satisfy the elastodynamic equations, the Fourier coefficients  $D_n(t)$  and  $F_n(t)$  are related by:

$$F_n(t) = -\frac{\mu |k_n|}{2} D_n(t) + \frac{\mu |k_n|}{2} \int_0^t W(|k_n| ct') \dot{D}_n(t-t') dt', \quad (4.4)$$

$$\dot{D}_n(t) = \frac{dD_n(t)}{dt}, \quad (4.5)$$

$$W(p) = \int_0^\infty \left[ \frac{J_1(\xi)}{\xi} \right] d\xi, \quad \text{with } W(0) = 1, \quad (4.6)$$

where  $J_1(\xi)$  is the Bessel function of order 1. The first term in equation (4.4) represents the static redistribution of stress after a certain amount of slip, while the second term captures the wave-mediated stress transfer. This term depends on slip rate and its history, and it is computed in the time interval of the length  $T_w$  for which the elastodynamic effect are considered. We called equations (4.1-4.6) the fully dynamic formulation.  $T_w$  is of the order of the time needed for the waves to propagate through the entire fault (further details about the convolution truncation can be found in *Lapusta et al.* (2000)). Relative to the fully-dynamic formulation, the quasi-dynamic models ignore this transient wave-propagation effect that influences the rupture (e.g., enhancing the stress concentration at the rupture tip). Equations (4.1-4.6) with  $T_w = 0$  (no convolution) correspond to the quasi-dynamic procedure of *Rice* (1993), *Ben-Zion and Rice* (1995) and *Rice and Ben-Zion* (1996). They lead to the static calculation of stress transfers but account for dynamic radiation away from the fault through the radiation damping term; that is why those models are described as quasi-dynamic procedures. Then, the stress-transfer functional  $f(z, t)$  for the quasi-dynamic models

can be expressed as follows:

$$f(z, t) = \sum_{n=-N/2}^{N/2} -\frac{\mu |k_n|}{2} D_n(t) e^{ik_n z}, \quad k_n = \frac{2\pi n}{\lambda}. \quad (4.7)$$

Note that, with no damping term  $\mu V/(2c_s)$  the quasi-dynamic procedure would turn into a quasi-static one and it would not allow solutions to exist during inertially controlled slip (*i.e.*, fast seismic slip). In the quasi-static formulation the slip rates become infinite as the seismic event approaches.

#### 4.2.2 Standart logarithmic rate-and-state laws

Laboratory-derived rate-and-state laws (*Dieterich, 1979; Ruina, 1983; Dieterich, 2007*, and references therein) have been successfully used to simulate the fault in its entirety, from the nucleation process to the dynamic rupture propagation, followed by postseismic slip, interseismic period and re-strengthening of the fault between earthquakes (*Lapusta et al., 2000; Noda and Lapusta, 2010; Kaneko et al., 2010; Noda and Lapusta, 2013*). We first adopt the laboratory-derived rate-and-state laws with the aging law proposed by *Dieterich (1979); Ruina (1983)* which assumes constant normal stress  $\sigma$ :

$$\tau = \bar{\sigma} f = (\sigma - p) \left[ f_0 + a \ln \left( \frac{V}{V_0} \right) + b \ln \left( \frac{V_0 L}{\theta} \right) \right], \quad (4.8)$$

$$\frac{d\theta}{dt} = 1 - \frac{V\theta}{L}, \quad (4.9)$$

where  $\tau$  is the shear stress,  $f$  is the friction coefficient,  $V$  is the slip velocity,  $p$  is the pore pressure,  $\theta$  is the state variable,  $L$  is the characteristic slip for state variable evolution,  $f_0$  is the value of the friction coefficient corresponding to the reference slip rate  $V_0$  and  $a > 0$  and  $b > 0$  are the constitutive parameters. At constant slip velocity  $V$ , the shear stress  $\tau$  and the state variable  $\theta$  evolve to their steady state values  $\tau_{ss}$  and  $\theta_{ss}$  respectively:

$$\theta_{ss}(V) = \frac{L}{V}, \quad (4.10)$$

$$\tau_{ss} = (\sigma - p) \left[ f_0 + (a - b) \ln \left( \frac{V}{V_0} \right) \right]. \quad (4.11)$$

Hence, the value of the parameter combination  $(a - b)$  defines the fault behavior at steady-state:  $(a - b) > 0$  corresponds to velocity-strengthening friction properties, which lead to stable slip with the imposed loading rate, while  $(a - b) < 0$  defines potentially seismogenic velocity-weakening regions of the model. We further refer to velocity-strengthening or velocity-weakening regions with the implicit understanding that this is the steady-state behavior.

Equation (4.8) is not defined for  $V = 0$ . To remedy this issue, we use the regularization following the physically-based approach based on an Arrhenius activated rate process describing creep at asperity contacts (*Lapusta et al.*, 2000; *Rice et al.*, 2001, and references therein):

$$\tau = \bar{\sigma}f(V, \theta) = (\sigma - p)f(V, \theta), \quad (4.12)$$

$$f(V, \theta) = a \sinh^{-1} \left[ \frac{V}{2V_0} \exp \left( \frac{f_0 + b \ln(V_0 \theta / L)}{a} \right) \right]. \quad (4.13)$$

### 4.2.3 Additional coseismic weakening

The standard logarithmic rate-and-state law has been derived from laboratory experiments at relatively low slip velocity, from  $10^{-9}$  to  $10^{-3}$  m/s, and small slips (of order centimeters) (*Dieterich*, 1979; *Ruina*, 1983). At seismic slip velocity of the order of 1 m/s, additional weakening mechanism can contribute. Several of the proposed additional processes are related to shear heating that unavoidably occurs during fast sliding that accumulates significant slip. With flash heating, fault gouge grains heat up at asperity contacts and substantially weaken, a phenomenon that has both theoretical and experimental support (e.g. *Lim and Ashby*, 1987; *Lim et al.*, 1989; *Tsutsumi and Shimamoto*, 1997; *Molinari et al.*, 1999; *Rice*, 1999; *Goldsby and Tullis*, 2002; *Beeler et al.*, 2008; *Rice*, 2006; *Tullis and Doldsby*, 2003; *Goldsby and Tullis*, 2011, and references therein). If the shear strain rate is sufficiently high, flash heating can occur even for small slip on the fault plane (of the order of 100 microns). Hence this mechanism might influence even the smallest earthquake. Pore fluid pressurization is another shear-heating-related weakening mechanism that might take place during seismic slip (e.g. *Sibson*, 1973; *Lachenbruch*, 1980; *Mase and Smith*, 1987; *Rudnicki and Chen*, 1988; *Sleep*, 1995; *Andrews*, 2002; *Bizzarri and Cocco*, 2006a,b; *Rice*, 2006; *Noda and Lapusta*, 2010). In that case, pore fluid expands faster in the shearing layer than the surrounding porous space, which increases the pore fluid pressure and hence decreases the effective normal stress, unless counteracted by fluid escape from the shearing zone and other potential processes such as inelastic dilatancy. Other suggested weakening processes include frictional melting (e.g. *Tsutsumi and Shimamoto*, 1997; *Hirose and Shimamoto*, 2005), dynamics of sliding between dissimilar materials (e.g. *Andrews and Ben-Zion*, 1997; *Adams*, 1998; *Cochard and Rice*, 2000), gel formation (*Goldsby and Tullis*, 2002; *Di Toro et al.*, 2004), and elastohydrodynamic lubrication (*Brodsky and Kanamori*, 2001).

For the purpose of this study, we incorporate the effect of flash heating only. The logarithmic rate and state formulation at steady state (4.11) is modified to (*Noda and Lapusta*, 2010; *Lapusta et al.*, 2013):

$$f_{ss}(V) = f(V, \theta_{ss}(V)) = \frac{f(V, L/V) - \text{sign}(V)f_w}{1 - \text{sign}(V)V/V_w} + \text{sign}(V)f_w, \quad (4.14)$$

$$\text{with } \frac{d\theta}{dt} = \frac{V\theta_{ss}(V)}{L} - \frac{V\theta}{L} = \frac{V}{L} (\theta_{ss}(V) - \theta), \quad (4.15)$$

where  $V_w$  is the characteristic slip velocity at which flash heating becomes significant (Figure 4.1b) and  $f_w$  is the residual friction coefficient. Based on laboratory experiments and flash heating theories,  $V_w$  is of the order of 0.1 m/s. Selecting much larger values of  $V_w$  would effectively disable the additional weakening due to flash heating and it would be equivalent to the formulation with the standard but regularized rate-and-state laws (equations 4.12-4.13).

#### 4.2.4 Fault geometry and computational procedures

Fault geometry and properties in our simulations have been selected to follow *Kaneko et al.* (2010) study for comparison purposes (Figure 4.1c and Table 4.1). The fault is therefore 240 km long, subdivided into three VS segments (80 km each on both sides and 15 km in the middle), that surround two VW regions each 72.5 km long. The length of the central VS segment is varied in our simulations. We assign the rate-and-state parameter as follows:  $a$  is 0.01 for the entire fault and  $b$  varies to define VS and VW areas.  $b$  is 0.015 in the VW regions and -0.01 and 0.008 for VS segments on the side and in the middle respectively. Uniform time-independent effective normal stress  $\bar{\sigma} = (\sigma - p) = 50$  MPa is applied on the entire fault. The reference slip velocity  $V_0 = 10^{-6}$  m/s, characteristic slip distance  $L = 8$  mm, Poisson's ratio  $\nu = 0.25$ , and shear wave speed  $c_s = 3.3$  km/s are also constant over the fault. The fault is loaded from the sides by steady motion at the long-term slip rate  $V_{pl} = 50$  mm/yr. In the case of additional weakening, we set  $V_w$  and  $f_w$  to be 0.14 m/s and 0, respectively. The weakening is disabled in the VS regions by assigning  $V_w = 10^9$  m/s.

In simulations with the standard rate-and-state law, the shear prestress  $\tau_0$  is equal to that of *Kaneko et al.* (2010), which is 26.1 MPa for the VS patches on both sides of the fault, 28.2 MPa for the VS patch in the middle and two different values for the VW areas (28.5 MPa for the left one and 28.8 MPa for the right one) so that nucleation of the first earthquake preferentially starts at one side (left) rather than at the two sides at the same time (Figure 4.1). In the case of simulations with additional weakening, we apply different  $\tau_0$  to avoid getting large slips in the very first event. Indeed, the shear stress history (Figure 4.2) shows that, in the case of additional weakening, earthquakes nucleate at lower average stress than for the regular rate-and-state law. Therefore, to be closer to the long-term behavior, the following initial shear stress values have been applied for the cases with enhanced weakening: 23.6 MPa for the VS areas on the sides, 29.4 MPa for the central VS patch, and 9 MPa for the VW segment.

The reference friction coefficient  $f_0$  is set to be 0.6 everywhere, except for the simulations with additional weakening, where we use  $f_0$  to define a nucleation-prone patch. At the boundary between

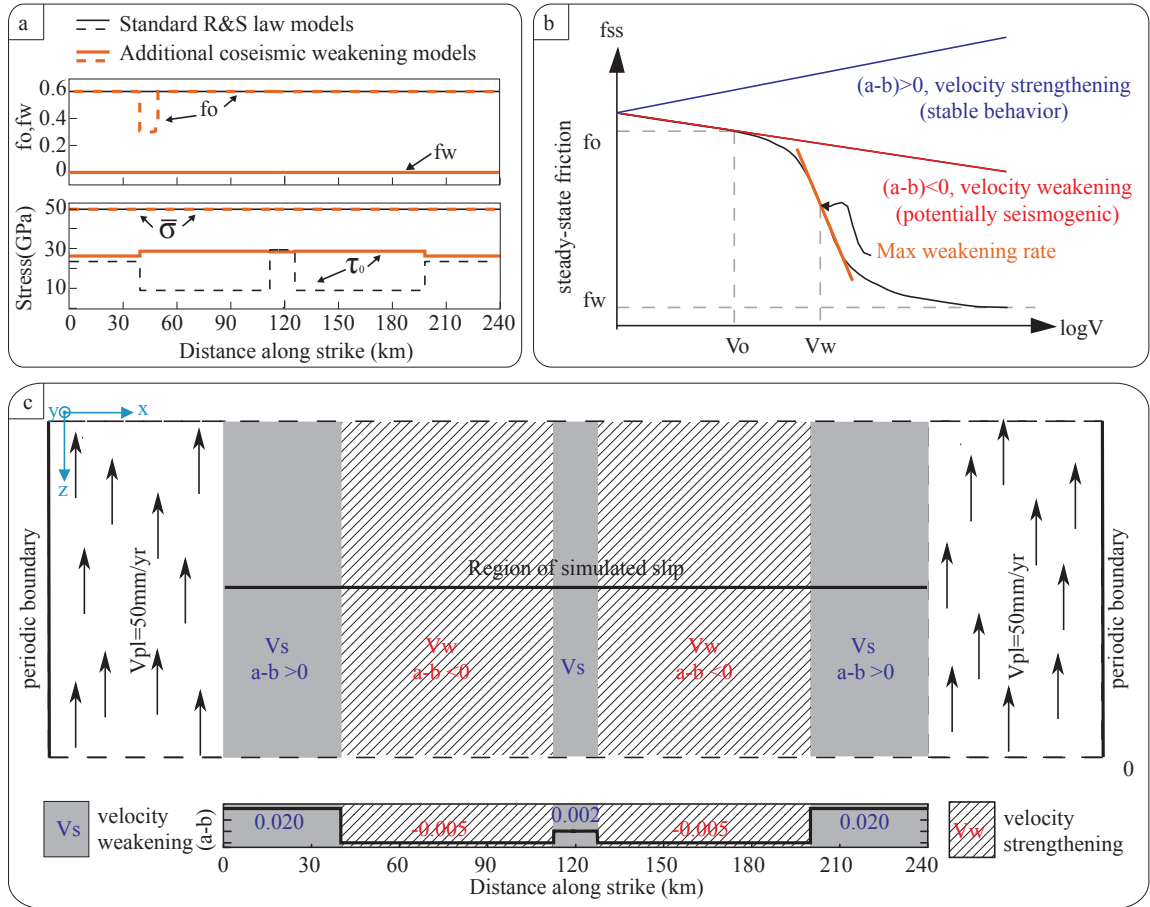


Figure 4.1: Schematics and parameters of the simulated fault. (a) Along-strike distribution of the reference friction coefficient ( $f_0$ ), residual friction coefficient ( $f_w$ ), effective normal stress ( $\sigma$ ), and initial shear stress ( $\tau_0$ ). Values for the standard rate-and-state law models are plotted in black while parameters for models with additional coseismic weakening are displayed in orange. (b) Schematics showing the dependence of the steady-state friction coefficient on slip velocity in velocity-weakening (VW) areas for rate-and-state law models with (black) and without (red) flash heating. The blue curve illustrates the rate dependence of velocity-strengthening (VS) segments. (c) Schematics of the simulated fault. Rate-and-state friction acts on the 240-km-long fault, subdivided into two VW and three VS segments. Fault is loaded from the sides by steady motion at the long-term slip rate  $V_{pl} = 50$  mm/yr. Along-strike variation of the friction parameter  $(a-b)$  is given for the main cases plotted in Figures 4.3 and 4.5. In the other cases, only the size and  $(a-b)$  value of the middle VS patch vary.

Parameter	Symbol	Value
Fault length along strike	$\lambda$	240 km
VW region length (total)	$W_{VW}$	145 km
VS region length (total)	$W_{VS}$	95 km
Loading slip rate	$V_{pl}$	50 mm/yr
Shear wave speed	$c_s$	3.3 km/s
Poission's ratio	$\nu$	0.25
Effective normal stress	$\bar{\sigma} = (\sigma - p)$	50 MPa
Reference slip velocity	$V_0$	$10^{-6}$ m/s
Reference friction coefficient	$f_0$	0.6
Rate-and-state direct effect	$a$	0.01
Rate-and-state parameters		
in VW regions	$b$	0.015
in VS regions	$b$	-0.01 / 0.008
Characteristic slip	$L$	8 mm
Residual friction coefficient	$f_w$	0
Characteristic slip velocity	$V_w$	0.14 m/s
Cell size	$\Delta x$	29 m

Table 4.1: Parameters for our simulations

VS and VW regions, continuous creep in VS segments concentrates the shear stress, promoting nucleation near these rheological transitions. For simulations with flash heating, we create on a 10 km weaker patch next to the boundary between the VS and VW regions, where  $f_0$  is decreased to 0.3 (Figure 4.1a). This weaker patch promotes earlier nucleation and therefore leads to more pulse-like ruptures. In our study, the weaker patch helps to get less unrealistic seismic events for QD simulations with additional weakening (section 4.4).

## 4.3 Simulations of earthquake sequences with standard R&S law: FD vs QD

### 4.3.1 Fault response: common features

Histories of slip for representative QD and FD simulations with standard rate-and-state law are displayed in Figure 4.3. Accumulation of slip during interseismic periods is represented by blue lines, which are plotted every 50 years. Red lines display cumulative slip every 2 seconds when the maximum slip velocity on the fault exceeds 1 mm/s, illustrating the end of earthquake nucleation and slip during seismic events.

Despite their relatively simple geometry and distribution of friction properties, the numerical models produce realistic complex fault behavior. They both show seismic and aseismic slip including transients. As expected from stability properties of fault with rate-and-state law (e.g., *Rice and Ruina*, 1983), the VS areas are steadily slipping at the slip rate comparable to the plate veloc-

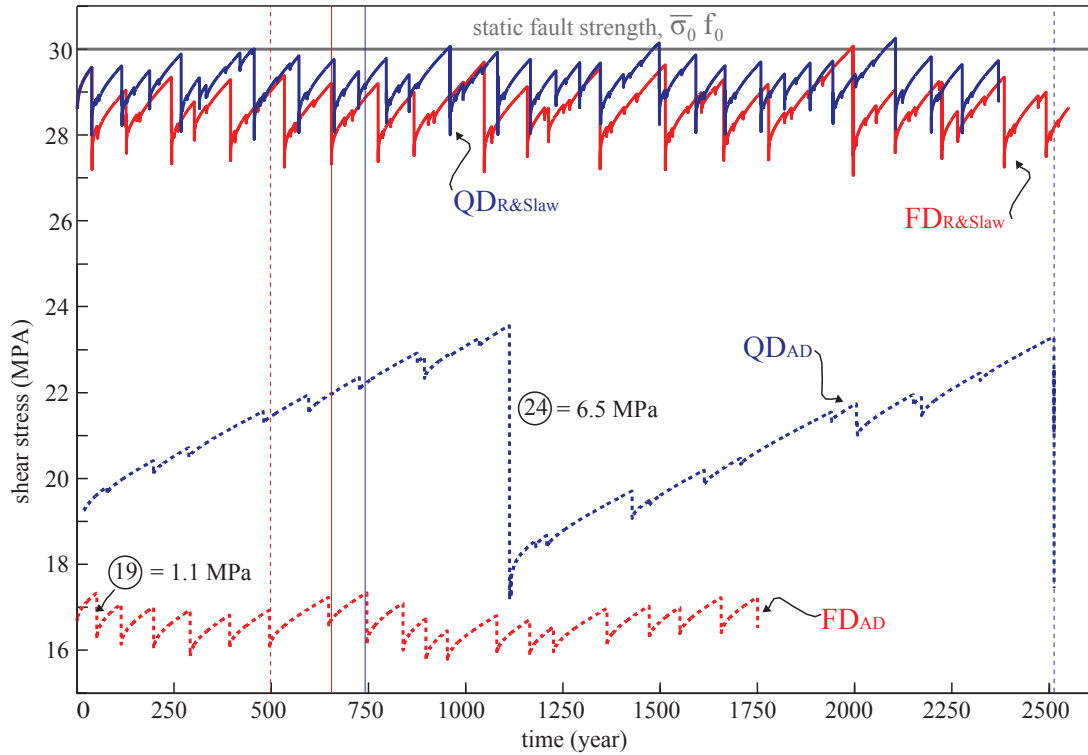


Figure 4.2: Shear stress levels on the fault over many earthquakes. The solid curves correspond to the QD (blue) and FD (red) standard rate-and-state (R&S) simulations. The corresponding vertical lines show the time limit for which we plot accumulation of slip on the fault in Figure 4.3. The dashed lines represent the stress levels for the QD (blue) and FD (red) simulations with additional coseismic weakening. Similarly, the corresponding vertical lines show the time over which we plot cumulative slip in Figure 4.5. The grey line gives a representative fault-averaged quasi-static fault strength ( $\bar{\sigma}_0 f_0$ ). In both cases (FD and QD), for the standard R&S law simulations, the average fault prestress before large, fault-spanning events is close to the representative static fault strength. In contrast, when models account for flash heating, the average fault prestress is significantly below the static fault strength, particularly for the FD case.

ity, whereas VW regions are almost fully locked during interseismic periods and accumulate the slip mainly during seismic events. Earthquakes nucleate where the fault undergoes local stress concentrations due to either rheological transitions from VS to VW regions or arrest of previous earthquakes. Depending on the level of prestress caused by previous slip, some events remains small, rupturing only a fraction of the VW area, while others grow large and propagate through the middle VS barrier. The larger VS regions on both sides of the model act as permanent barriers and coseismic ruptures penetrate into them only a little. The central VS patch affects rupture propagation, as shown by *Kaneko et al. (2010)*: sometimes it acts as a barrier, and sometimes coseismic rupture goes through. The behavior depends on a number of factors, as discussed in *Kaneko et al. (2010)* and section 4.6. When only one VW segment ruptures, static stress increases at the tip of the previous rupture area, promoting propagation of the subsequent event through the VS patch and leads to the stress transfer into the neighbouring VW segment. This often leads to the nucleation of another event, shortly after the first one, at the boundary between the central VS patch and the unruptured VW area, which is a type of clustering.

### 4.3.2 QD vs FD: differences

The QD and FD simulations also exhibit important quantitative and qualitative differences. The first observation is that the final slip is smaller in the QD case than for the FD simulation. As a consequence, fewer events are needed in the FD case to accumulate the same amount of slip. Furthermore, the rupture speed and slip velocity, which are related to the horizontal and vertical spacing of red lines, respectively, are much lower for the QD simulation than for the FD one. If we compute the average rupture speed between black arrows in Figure 4.3, we find 3.56 km/s and 0.98 km/s for the FD and QD simulation respectively. This phenomenon is also illustrated in Figure 4.4a, which display the maximum sliding velocity recorded during one event. These differences have already been pointed out by *Lapusta et al. (2000)* and *Lapusta and Liu (2009)*.

To quantify the evolution of the stress state on the fault for the two models, we consider the average shear stress  $\tau_{av}(t)$  defined as follows:

$$\tau_{av}(t) = \frac{1}{z_2 - z_1} \int_{z_1}^{z_2} \tau(z, t) dz, \quad (4.16)$$

where the spatial integration is taken over the VW regions plus the central patch, excluding the VS areas on the sides. Therefore,  $z_1 = 40$  km and  $z_2 = 200$  km for the two examples shown in Figure 4.3 (see Figure 4.1 for fault geometry). The time evolution of the average stress for the standard rate-and-state laws is plotted in Figure 4.2 with solid curves. The vertical solid lines correspond to the time limit for which the accumulation of slip on the fault in shown in Figure 4.3. The variations in the average shear stress display steady interseismic accumulation of stress due to the tectonic

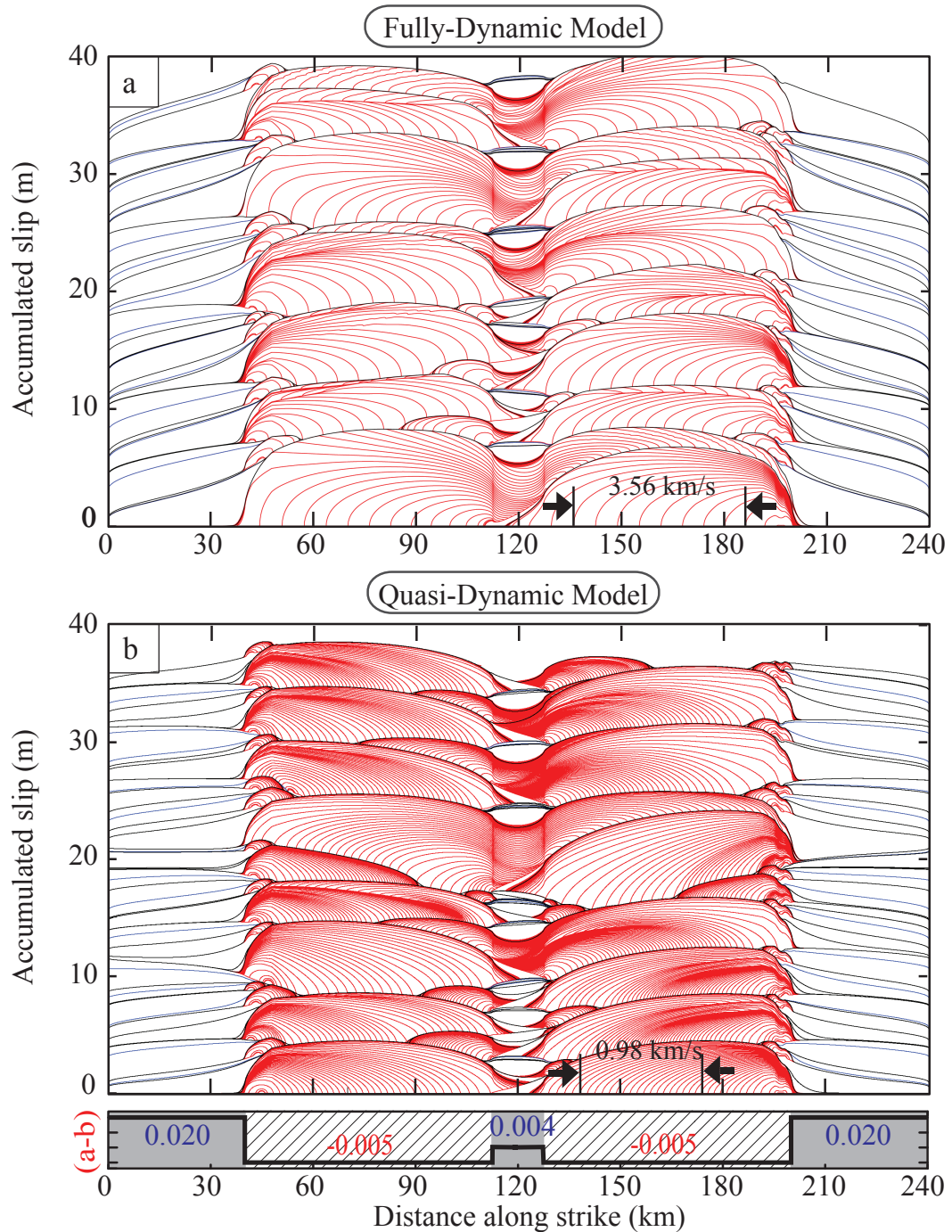


Figure 4.3: Cumulative slip on the fault for (a) FD and (b) QD simulations with the standard rate-and-state law. Red lines are plotted every 2 s during seismic events, when the maximum slip velocity exceeds 1 mm/s, while blue lines (every 50 years) illustrate the aseismic behavior of the fault. Black lines represent the cumulative slip after each seismic event. The middle VS patch creates complexity in both FD and QD cases. The FD events are bigger in general, display higher rupture speed (computed between black arrows), and are more likely to rupture the middle VS asperity as discussed in section 6.

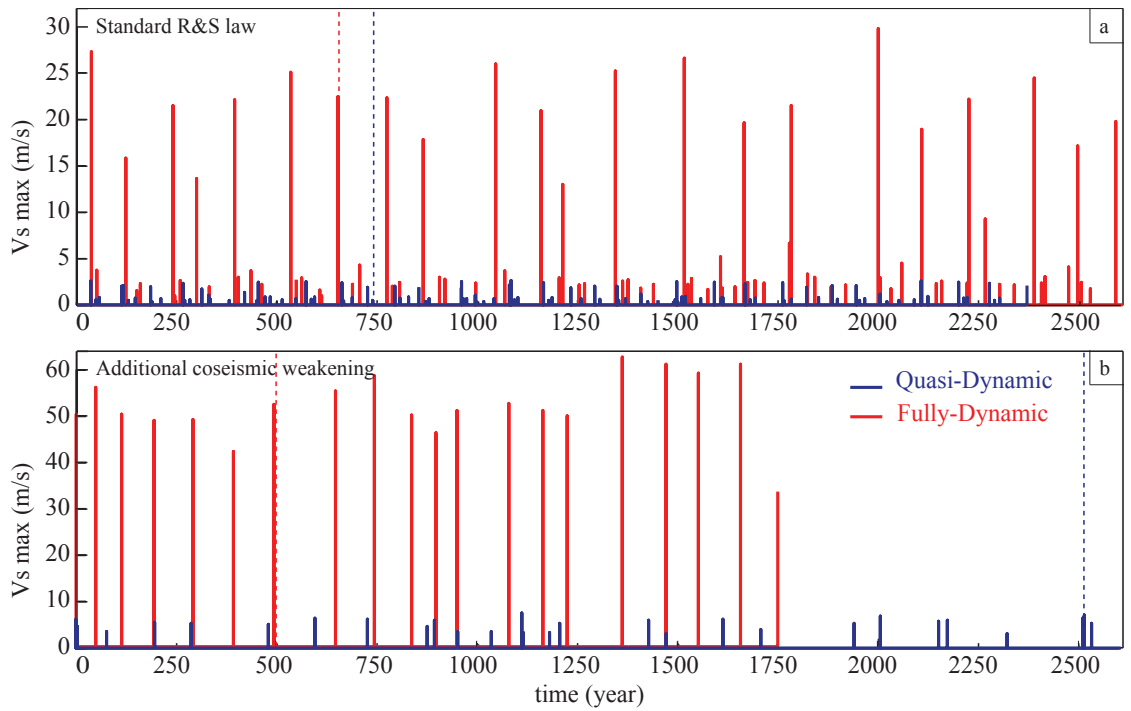


Figure 4.4: The maximum slip velocity over the fault for the QD and FD simulations (a) without and (b) with additional coseismic weakening for the reference cases plotted in Figures 4.3 and 4.5, respectively. In both cases, the maximum velocity is much higher (about 10 times) in the FD simulations than in the QD ones. Accounting for additional coseismic weakening also increases significantly the slip velocity (about 2 times) for both QD and FD formulations but the ratio between the two stays similar. The vertical dashed lines illustrate the time limit for which we plot the cumulative slip on the fault in Figures 4.3 and 4.5.

loading, with occasional abrupt drops representing the simulated earthquakes. Consequently, local peaks of the average shear stress correspond to the level of stress on the fault before earthquakes nucleate. For both curves, the peaks are close to the representative quasi-static (or low-velocity) fault strength  $\bar{\sigma}f_0 = 30$  MPa (the grey line in Figure 4.2) averaged over the seismogenic part of the fault (VW segments + VS asperity), but the FD simulation displays a slightly smaller value compared to the QD model. This shows that the FD formulation promote the nucleation, with the wave-mediated stress transfer enhancing the stress concentration in the nucleation zone and promoting the transition to rapid expansion at lower values of prestress. If one divides the shear stress peak values by the effective normal stress (50 MPa) to estimate the equivalent friction coefficient, one finds a value of 0.55 for the QD simulation and 0.54 for the FD case, which is close to the representative quasi-static friction coefficient ( $f_0 = 0.6$ ). The stress drop for the larger events is, on average,  $\sim 0.99$  MPa and  $\sim 1.26$  MPa for the QD and the FD simulations, respectively, which is consistent with the difference in the cumulative slip per event observed in Figure 4.3. Note that we estimate the stress drop directly from the fault-averaged shear stress change from Figure 4.2. Such fault-averaged stress is not exactly equal to the seismologically estimated moment-based stress drop (*Noda and Lapusta, 2013*). However, for the relatively uniform slips that we have in our models, the two estimates are quite close.

Overall, the FD and QD models in the case of standard rate-and-state law are qualitatively similar but quantitatively different. We will see in the following section that the differences are much more dramatic in the presence of enhanced coseismic weakening.

It has been hypothesized (*Lapusta et al., 2000*) that smaller radiation damping terms in the QD formulation can make the comparison with FD models more favourable. In that case, constant  $\beta_s$  is added to equation (4.1):

$$\tau(z, t) = \tau^0(z, t) + f(z, t) - \frac{\mu}{2c_s\beta_s}V(z, t), \quad (4.17)$$

with  $\beta_s \geq 1$ . *Lapusta and Liu (2009)* have explored this hypothesis for 3D cases and found that indeed, the rupture speed in the QD simulations increases with the higher values of  $\beta_s$ , however, the slip velocity remains small in comparison with the FD events. Moreover, final slip, average slip per event, and static stress drop are smaller for all the QD simulations they have explored ( $\beta_s = 1, 2$  or  $4$ ). *Lapusta and Liu (2009)* also emphasized that increasing  $\beta_s$  further is not a promising approach, since the rupture speed for  $\beta_s = 4$  is already higher than that in the FD case. Therefore, the QD approach can be used to explore the fault behavior qualitatively in some cases (see section 4.7 for more discussion) but it cannot be precise quantitatively.

## 4.4 Simulations of earthquake sequences with additional weakening: FD vs QD

### 4.4.1 Fault response : seismic and aseismic slip including transient

Despite having the same model parameters, QD and FD simulations display drastic differences in cases with additional dynamic weakening. Slip history for representative QD and FD simulations is displayed in Figure 4.5. As for Figure 4.3, the accumulation of slip during the interseismic period is plotted every 50 years in blue, whereas the accumulation of slip during seismic events is displayed every 2 s with red lines. For plotting purposes, we increase four times the ordinate axis for the QD simulation, but we keep the same scale as in Figure 4.3 for the FD case. Both FD and QD simulations show seismic and aseismic slip, including transients, but earthquake ruptures are very different in size, recurrence, and propagation mode.

The first observation is that earthquake events can become unrealistic in the QD simulation if the friction law includes coseismic weakening mechanisms. For example, event 24 in the QD model (Figure 4.5) displays a maximum slip of 75 m while FD simulations records  $\sim 6$  m of slip on average with the peak at 7 m. Moreover, despite the simple geometry and the same parametrization, QD simulations produce a more complex earthquake sequence behavior. In the FD model, for this particular setup, all events are able to propagate through the VS region in the middle and look very similar to one another. In the QD solution, depending on the level of prestress, some events remains small, rupturing only a fraction of the VW area, while others grow large and propagate through the middle VS barrier (Figure 4.5).

### 4.4.2 Pulse-like ruptures in FD vs crack-like ones in QD simulations

The mode of rupture for the largest events in the two simulations are radically different: the FD solution generates pulse-like events, while the QD formulation results in crack-like events. To illustrate this phenomenon, Figure 4.5 shows in grey the spatial extend of fault slipping during 2 sec interval, close to the end of the rupture. For event 19 in the FD simulation, only a small part of the fault ( $\sim 10$  km out of 160 km) slips during those 2 sec, while in the QD simulation (event 24), the slipping area is 140 km out of 160 km, with most of the seismogenic part of the fault slipping. We see that, for the QD cases, the region where the earthquake nucleated keeps slipping as the rupture propagates further.

Evolution of slip rate through time for the two events is another way to emphasize the difference (Figure 4.6 for the FD event 19 and Figure 4.7 for the QD event 24). Both seismic events nucleate similarly, but thereafter they display a very different story. In the FD dynamic case (Figure 4.6), while propagating through the VW area, the slipping region is consistently narrow and the second

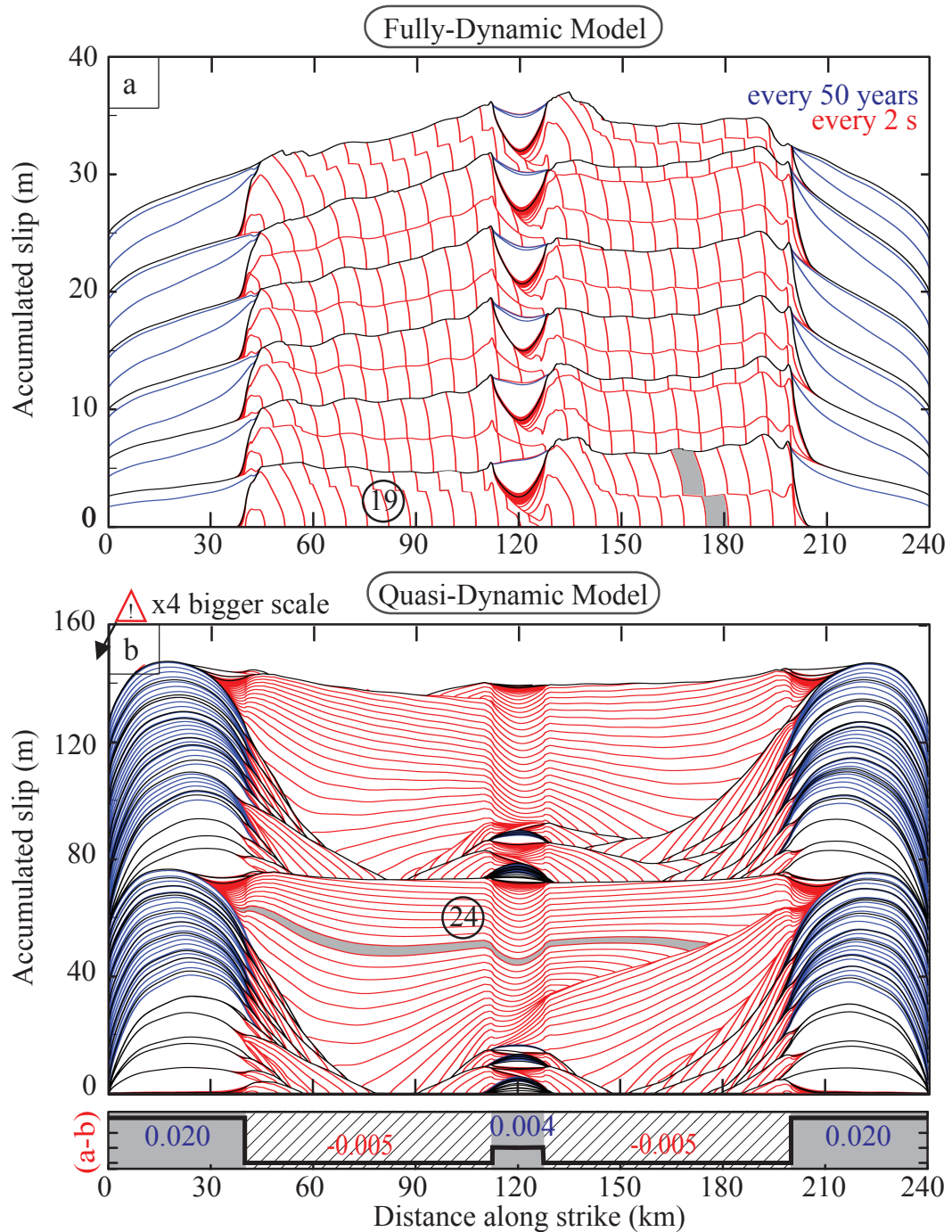


Figure 4.5: Cumulative slip on the fault for the a) FD and (b) QD simulations with the rate-and-state law and additional coseismic weakening. Note that the y-axis has four times larger values in (b) than in (a). Red lines are plotted every 2 s during seismic events while blue lines are plotted every 50 years. Black lines represent the cumulative slip after each seismic event. The FD and QD events are very different in size, recurrence, and propagation mode. The FD solution generates pulse-like events, while the QD formulation results in smaller events in the form of dying pulses and large crack-like events. The slip-rate snapshots for events 19 in (a) and 24 in (b) are displayed in Figures 4.6 and 4.7, respectively.

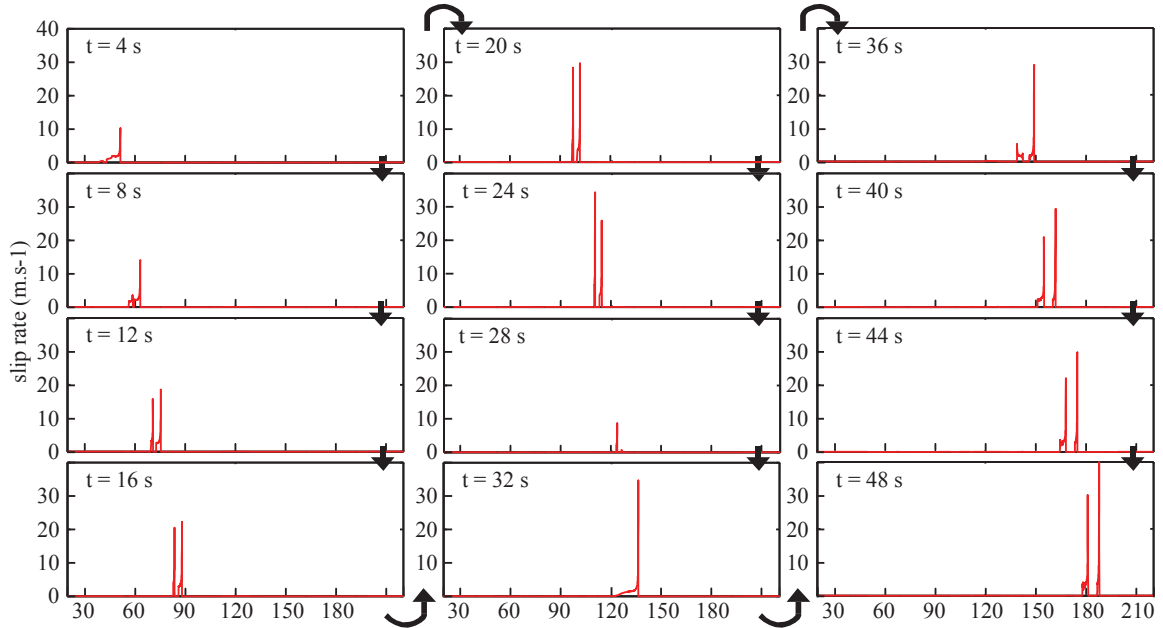


Figure 4.6: Snapshots of slip rate on the fault for a representative FD event with enhanced coseismic weakening. The slip rate is non-zero only on a small portion of the fault at a time, indicating that the rupture propagates as a narrow self-healing slip pulse (which is actually a double pulse in most snapshots). The slip rate increases as the rupture propagates through the first (right) VW segment, but then decreases when the rupture encounters the VS middle patch. Propagation in the second VW patch leads to the slip rate increasing again. For the cumulative slip history of this seismic event (number 19), see Figure 4.5.

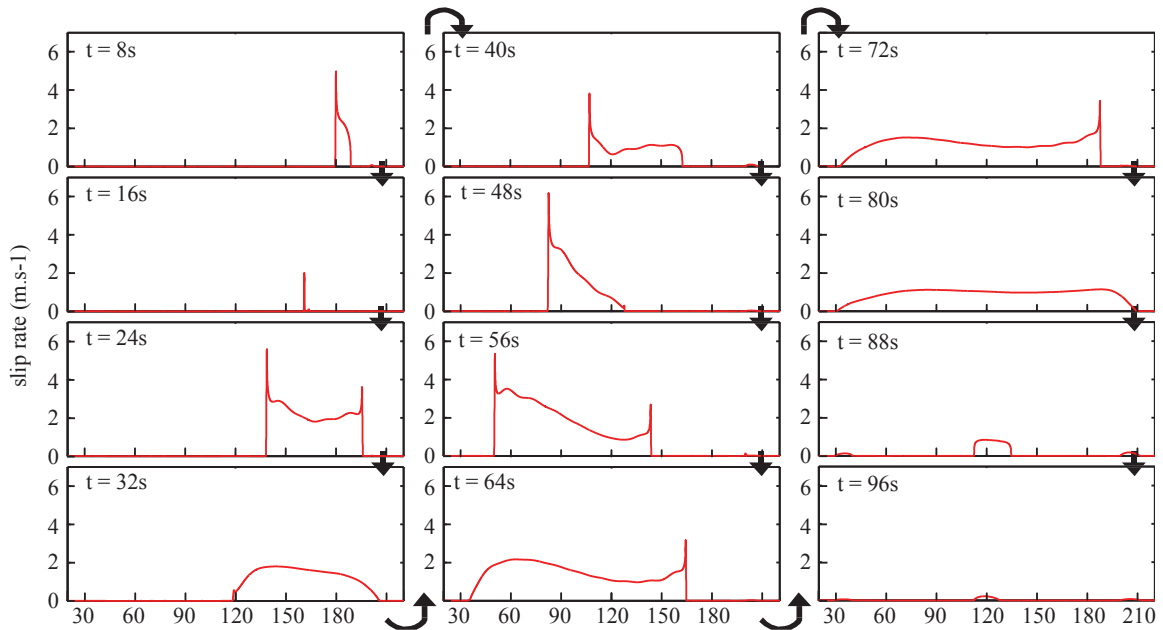


Figure 4.7: Snapshots of slip rate on the fault for a representative model-spanning QD event with enhanced coseismic weakening. As the rupture propagates through the fault, segments that have already sustained seismic motion still accumulate more slip, which leads to the development of a crack-like rupture. The middle VS patch decreases the slip rate but does not stop the rupture. For the cumulative slip history of this seismic event (number 24), see Figure 4.5.

pulse is developed ( $t = 8$  s to  $t = 29$  s). When the rupture encounters the central VS patch ( $t = 28$  s), the slip rate drastically decreases. Propagation in the second VW patch leads again to the creation of a double pulse and slip rate increases up to 40 m/s. For the QD event number 24 (Figure 4.7), nucleation starts within the right VW region, then the rupture extends bilaterally in a crack-like modes. The rupture becomes less vigorous as it propagates through the central VS patch, then re-surges on the other side, with large slips that promote the re-rupturing of the right VW patch.

Note that the smaller events in the QD case, the ones that nucleate at the sides of the seismogenic region and arrest before reaching the middle of the fault, propagate as dying pulses.

#### 4.4.3 Average shear stress level on the fault

The state of stress on the fault is strongly influenced by the FD vs QD modeling procedures. The time evolution of average shear stress (equation 4.16) for the QD and FD models with additional weakening mechanisms is plotted in Figure 4.2 with the dashed blue and red curves, respectively. The corresponding vertical lines show the time limit for which the accumulation of slip is illustrated (Figure 4.5). Unlike for simulations that assume the standard rate-and-state logarithmic-type coseismic weakening, the average shear stress on the fault with additional coseismic weakening is much smaller than the quasi-static strength  $\bar{\sigma}f_0$ . Accounting for full inertial effects reduces even more the average stress level. In the simulation with additional weakening and wave-mediated stress transfers (dashed red curves), the peaks of the average shear stress are between 16.5 and 17.3 MPa, with the equivalent friction coefficients of 0.33 and 0.35, respectively. The seismic events are very similar, with the return period of  $\sim 92$  years on average and stress drop of  $\sim 0.78$  MPa. The QD simulation displays a very different behavior. Interseismic increase of average shear stress, punctuated by stress drop due to smaller events, is observed over a period of  $\sim 1100$  years until the stress reaches a peak of 23.6 MPa. During that time, smaller events can occur on the sides of the fault and their stress drops appear smaller on this plot due to averaging over the entire fault. The equivalent coefficient of friction in this QD case is close to 0.47. Thereafter, the fault records a large event with the stress drop of 6.5 MPA, 8.3 times bigger than that of a representative FD event (Figure 4.2).

### 4.5 Reasons for the dramatic differences between FD and QD simulations with enhanced weakening

It is clear that the QD simulations produce qualitatively different outcome from the FD ones in the cases with enhanced coseismic weakening, unlike our findings for the models with standard rate-and-state weakening only, as in section 4.3. In all cases, the exclusion of the wave-mediated stress transfers lowers stress concentration at the rupture tip, hence lowering slip rates there. In

the case of the standard rate-and-state law, this mostly leads to slower rupture speeds, consistent with dynamic fracture mechanics (e.g., *Freund*, 1990); however, the amount of weakening the fault experiences is virtually unchanged, since the weakening in the standard rate-and-state friction laws is only logarithmically dependent on the slip rate. In the case of enhanced coseismic weakening, however, the dependence of fault weakening on the slip rates is much stronger, and the reduction of slip rates in the QD simulations has a profound effect on how the fault weakens with slip. In essence, the FD simulations have more intense fault weakening than the QD ones, promoting low-stress fault operation and pulse-like rupture mode as consistent with the previous theories and numerical findings (*Zheng and Rice*, 1998; *Noda et al.*, 2009; *Lapusta et al.*, 2013). As the result, the FD simulations have the fault operating under low overall prestress (section 4.4.3) with all ruptures propagating in the pulse-like mode (section 4.4.2), while the QD simulations produce a mixture of smaller events that arrest as dying pulses and much larger, model-spanning, crack-like ruptures under larger prestress.

The differences between the FD and QD simulations manifest themselves even during the nucleation processes. As mentioned in section 4.2.4 for the simulations with additional weakening, the reference friction coefficient  $f_0$  is defined to be 0.6 everywhere, except for the nucleation-prone patch near the transition zone between the VW and VS segments (at  $x \simeq 45$  km in Figure 4.1). In the FD models, all events nucleate at that particular location. In the QD simulations, events nucleate on both sides of the VW fault and even at the boundary with the VS barrier in the middle of the fault (Figure 4.5), while the weaker patch simply produces more numerous small events. This can be linked to the level of stress at which events are able to propagate, which varies in the two models. In both cases, earthquakes can nucleate in the nucleation-prone patch while most of the fault is far from its static strength. By the time the rupture reaches the statically stronger parts of the faults (where  $f_0 = 0.6$ ), it must be able to cope with the high mismatch between the prestress and the higher static strength of the fault to keep propagating. This is possible for the FD simulations, due to higher slip rates and associated more intense weakening, but not in the QD simulations that can only support the dying pulse-like and the crack-like mode. This is why we observe the interseismic average stress increases over a period of  $\sim 1100$  in the QD simulation (Figure 4.2), which brings the VW segments to a stress level closer to its quasi-static strength value.

## 4.6 Quantifying the effect of VS patches on seismic ruptures

As mentioned in the introduction, a important question in seismotectonics is the ability of the earthquake rupture to propagate over faults with heterogeneous properties. In particular, a case of seismogenic patches separated by creeping barriers has emerged as that of significant practical interest based on observations (e.g., *Burgmann et al.*, 2005; *Hetland and Hager*, 2006; *Chlieh et al.*,

2008; Perfettini *et al.*, 2010; Chlieh *et al.*, 2011; Loveless and Meade, 2011). Kaneko *et al.* (2010) explored the dependence of earthquake rupture patterns and interseismic coupling on spatial variations of fault friction using FD simulations. Here we consider the importance of accounting for full wave-mediated effects in modeling of that kind.

Following the study of Kaneko *et al.* (2010), we analyze the probability  $P$  of an earthquake to rupture the VS middle patch in QD dynamic simulations, to compare with the statistics computed for FD models. We start each simulation with arbitrary initial conditions (described in subsection 4.2.4) and then simulate the fault behavior for 10,000 years. Based on the study of Kaneko *et al.* (2010), the probability  $P$  is estimated from the percentage of earthquakes that propagate through the VS patch relative to the number of earthquakes that rupture entirely one or two of the VW segments (Kaneko *et al.*, 2010). Kaneko *et al.* (2010) identified a non-dimensional parameter,  $B$ , which correlates with the probability  $P$ . The parameter  $B$  relates the amount of stress that is needed by the VS patch to sustain the rupture and the amount of stress that the incoming rupture can provide to the VS patch. It is given by:

$$B = \frac{\Delta\tau_{prop}D_{vs}}{\beta\Delta\tau_{vw}D_{vw}}, \quad (4.18)$$

which can be approximated as:

$$B \simeq \frac{\ln(V_{vs}^{dyn}/V_{vs}^i)\bar{\sigma}_{vs}(a_{vs} - b_{vs})D_{vs}}{\beta\Delta\tau_{vw}D_{vw}}, \quad (4.19)$$

where  $\Delta\tau_{prop}$  is the stress required by the VS patch,  $D_{vs}$  and  $D_{vw}$  are the sizes of the VS patch and VW segment, respectively,  $\Delta\tau_{vw}$  is the average coseismic stress drop over the VW segment from which the rupture is attempting to enter the VS patch,  $\bar{\sigma}_{vs}$  is the normal stress in the VS patch,  $V_{vs}^{dyn}$  and  $V_{vs}^i$  are the seismic and pre-event (interseismic) velocity in the VS patch, respectively,  $a_{vs} - b_{vs} > 0$  is the velocity-strengthening parameter in the VS patch, and  $\beta$  is a model-dependent geometric factor that specifies the fraction of the stress transferred onto the VS patch; following Kaneko *et al.* (2010) we use  $\beta = 0.5$  for the 2D model considered here. As  $B$  increases from 0 to  $\sim 1$ , the percentage  $P$  drops from 100% to 0% (Kaneko *et al.*, 2010).

#### 4.6.1 Models with standard rate-and-state friction

For simulations with the standard rate-and-state law, the dependence of the propagation probability  $P$  on the parameters of the VS patch displays similar trends in the FD and QD simulations (Figure 4.8a and 4.8b). For both approaches, the higher the value of  $(a_{vs} - b_{vs})$  and/or the larger the size  $D_{vs}$ , the more efficient the patch is in stopping earthquake rupture, which is consistent with the prediction based on the parameter  $B$ . Moreover, if we look at the distributions of slip in individual events (cases Q1-3 and F1-3 in Figure 4.9), the overall rupture pattern is qualitatively similar.

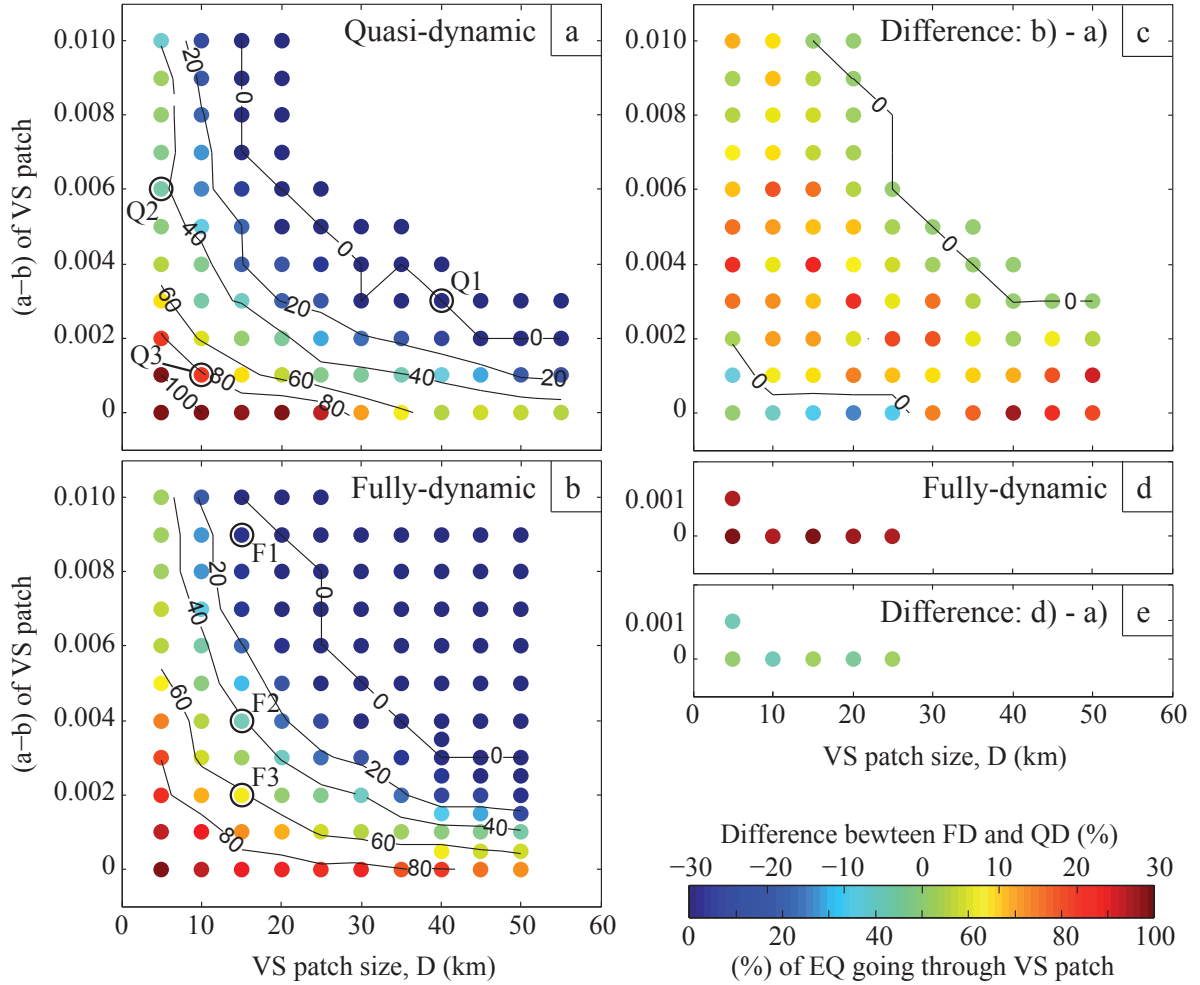


Figure 4.8: The ability of seismic ruptures to propagate through an unfavorable fault region in the form of a VS patch in simulations with the rate-and-state friction only. The relation between the properties of the VS patch and the probability  $P$  (in color) that an earthquake would propagate through it is shown for the (a) QD approach (this study) and (b) FD approach (modified from (*Kaneko et al.*, 2010)). Each colored dot corresponds to a 10,000-year simulation of fault slip with more than 50 events that rupture either one or both VW segments.  $P = 0\%$  means that the VS patch is a permanent barrier. Black lines are the isocontours of  $P$ . Slip distributions in seismic events for cases Q1-3 and F1-3 are displayed in Figure 4.9. (c) The difference in probability  $P$  between the QD and FD cases. (d) Several FD simulations recomputed with the same code and computational cluster as the QD simulations (see the text for more explanation). (e) The difference in probability  $P$  between the QD and FD cases from (d).

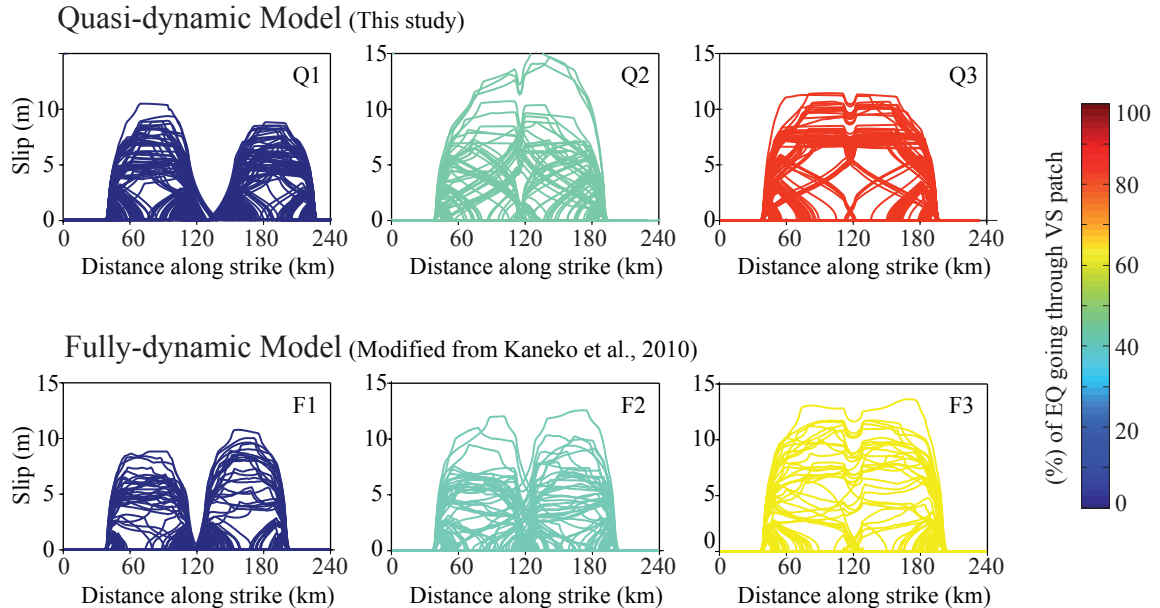


Figure 4.9: Slip distributions of the seismic events corresponding to cases Q1-3 (QD simulations) and F1-3 (FD simulations) from Figure 4.8, illustrating the range of fault behaviors that both QD and FD simulations can produce but not for the same properties of the VS region. The VS patch can either act as a permanent barrier (Q1 and F1) or let some of the earthquakes to propagate through (Q2-3 and F2-3).

Nevertheless, there are important quantitative differences. In the QD simulations, the VS patch acts as a permanent barrier for smaller values of  $(a_{vs} - b_{vs})$  and/or  $D_{vs}$  (Figure 4.8a) than in the FD simulations. Furthermore, for most cases in which the VS patch is a partial barrier, up to 30% more events propagate through the VS patch in the FD simulations that incorporate full inertial effects (Figure 4.8c). These results are likely due to two factors. First, the stress drop  $\Delta\tau_{vw}$  in equation 4.18 is higher for the FD simulations (Figure 4.2 and section 4.3.2), leading to smaller  $B$  and hence higher probability of propagation  $P$ . Second, incorporating all wave-mediated stress transfers - as in the FD simulations - leads to higher stress concentration at and in front of the rupture tip and hence promotes rupture propagation through unfavorable regions such as the VS patch. This latter effect is not completely accounted for by parameter  $B$  which is based on quasi-static consideration of stress transfer.

Note that, in the particular case of a velocity-neutral patch ( $(a_{vs} - b_{vs}) = 0$ ) and for another case where the velocity strengthening of the patch is small ( $(a_{vs} - b_{vs}) = 0.001$ ,  $D_{vs} = 5$  km), we observe the opposite trend: the QD formulation seems to slightly enhance rupture propagation through the patch (Figure 4.8c). Since our QD computations (Figure 8a) have been executed on a different computational cluster and with an updated code compared to the FD simulations of *Kaneko et al.* (2010), we first check whether there might be small computational differences between the two types of simulations. To that end, we redo the FD computations for the cases in question (Figure 4.8d) and

indeed find that the results are slightly different, by 0 to 5% in the propagation probability  $P$ . This is not surprising, since small differences in the order of the computational operations accumulate and can lead to rupture arrest or propagation over the VS patch in these highly nonlinear problems. Comparing the FD and QD calculations done with the same code on the same computational cluster, we still find that the QD simulations lead to slightly more ruptures propagating through the VS patch in some cases (e.g.,  $(a_{vs} - b_{vs}) = 0$ ,  $D_{vs} = 10$  km), although the difference is smaller, up to at most 5% (Figure 4.8e), while for some other cases (e.g.,  $(a_{vs} - b_{vs}) = 0$ ,  $D_{vs} = 15$  km), the FD simulations have a slight edge of up to 0.5%. Overall, these results imply that the difference between FD and QD simulations for rupture propagation over the velocity-neutral patch is near zero. This is consistent with our simulations without the patch, where large events, once they reach the middle of the fault, propagate to the other end of the fault in both FD and QD simulations, implying 100% propagation probability (recall that  $P$  is computed based only on those events that fully rupture one of the VW sides of the fault). The addition of a patch with properties close to the rest of the fault cannot change this behavior much, at least for relatively small patches, and the FD and QD simulations both have near-100% probability of propagation through the patch in those cases.

Overall, the effect of FD vs. QD simulations with the standard rate and state friction on the ability of rupture to propagate through an unfavorable patch is similar to the comparison discussed in section 3: the results are qualitatively similar but quantitatively different.

#### 4.6.2 Models with enhanced coseismic weakening

For the models with enhanced coseismic weakening, we explore a smaller representative subset of cases to shorten the computational time. We consider a 15-km-long VS patch with a range of velocity-strengthening  $(a_{vs} - b_{vs})$  values (Figure 4.10a).

As expected based on the results of section 4.4, the two simulation approaches display more dramatic differences in the models with enhanced coseismic weakening. For smaller values of  $(a_{vs} - b_{vs})$ , the large events still propagate through the patch in almost 100% in both cases, as in the models with the standard rate-and-state friction (section 4.6.1). However, the behavior deviates for larger values of  $(a_{vs} - b_{vs})$ . In the QD cases, the decrease in probability  $P$  is essentially gradual with  $(a_{vs} - b_{vs})$  and relatively slow, with about 50% of ruptures propagating through the VS patch for the largest value, 0.01, of  $(a_{vs} - b_{vs})$  explored. In the FD case, near-100% propagation persists until  $(a_{vs} - b_{vs}) \leq 0.005$ , and then the propagation probability  $P$  relatively rapidly drops, with the VS patch essentially becoming a permanent barrier for  $(a_{vs} - b_{vs}) \geq 0.008$ .

The differences between the rupture-patch interaction in the FD and QD simulations can be explained by the differences in the rupture propagation mode and size detailed in section 4.4. The FD simulations produce similar pulse-like ruptures that initiate on the side of the VW segment away from the patch, and attempt to propagate over the patch after entirely rupturing one of the VW

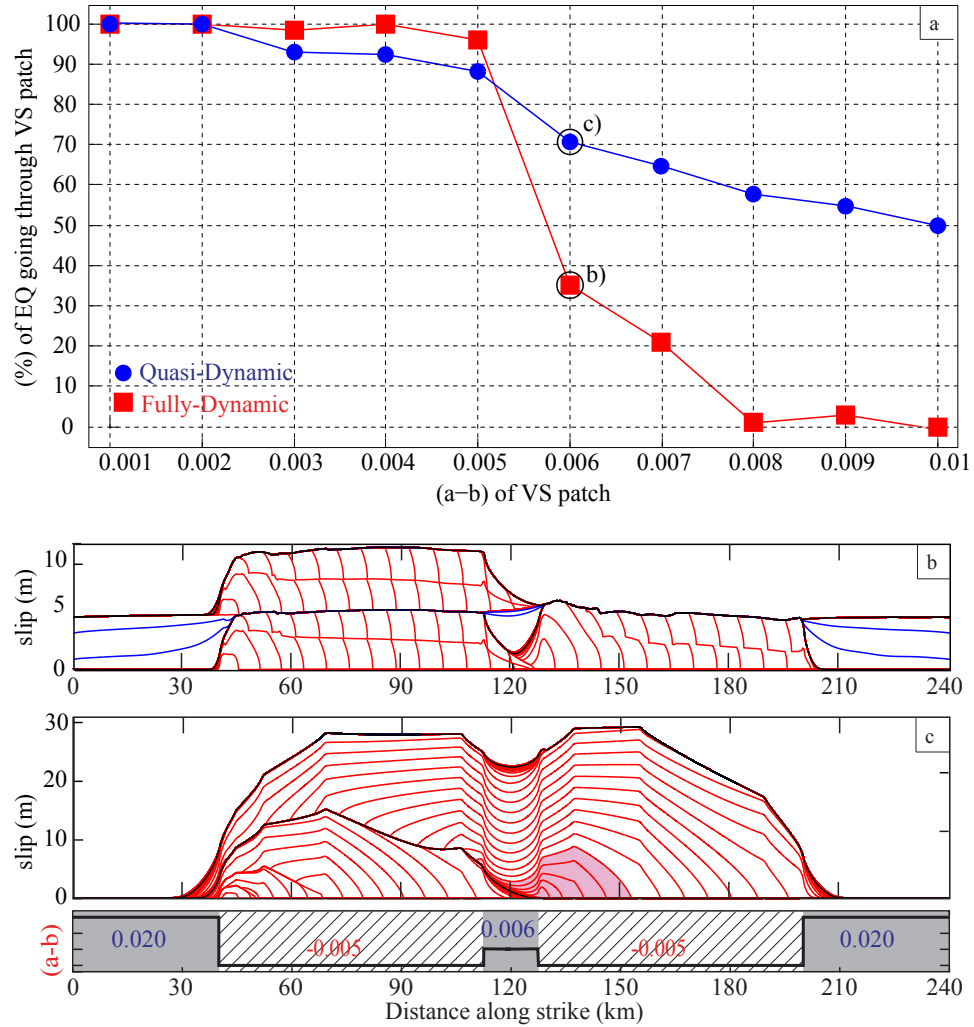


Figure 4.10: The ability of seismic ruptures to propagate through an unfavorable fault region in the form of a VS patch in simulations with additional coseismic weakening. (a) Probability  $P$  that an earthquake propagates through a 15-km patch is plotted against the friction parameter  $(a - b)$  of the patch. Each red squares correspond to a 10,000-year FD simulation of fault slip with more than 50 events that rupture either one or both VW segments. Events spanning the entire fault are more rare with the QD simulations (blue dots), therefore the QD statistics has been computed over at least 20 events that arrest at or propagate through the VS patch. The FD and QD results are quite different, as discussed in the text. (b) and (c): Cumulative slip on the fault for representative events in the FD and QD simulations, respectively, when  $(a_{vs} - b_{vs}) = 0.006$ . Red lines are plotted every 2 s during seismic events while blue lines are plotted every 50 years.

segments (e.g., Figure 4.5; Figure 4.10b). Such behavior results in a relatively stable value of  $\Delta\tau_{vw}$ , of about 3 MPa in our cases. Using this value in the approximate expression of  $B$ , equation 4.19, with the typical value of  $\ln(V_{vs}^{dyn}/V_{vs}^i) = 20$  (Kaneko *et al.*, 2010), and determining the value of  $(a_{vs} - b_{vs})$  that corresponds to  $B = 1$  results in 0.007. The value of  $(a_{vs} - b_{vs}) = 0.007$  is indeed close to the value of 0.008 at which the VS patch becomes a permanent barrier in the fully dynamic case (Figure 10). The decay of the probability over a range of  $(a_{vs} - b_{vs})$  values, from 0.005 to 0.008, is likely related to the variability of events and inter-event times - and hence values of  $\Delta\tau_{vw}$  and  $V_{vs}^i$  - observed in the FD simulations (Figures 4.5a and 4.2).

In the QD simulations, the larger events that attempt to break the VS patch nucleate at different distances from the VS patch, including right next to it, and hence are in a different state of their development when they reach the VS patch. This results in different relevant values of  $\Delta\tau_{vw}$  and effective ruptured  $D_{vw}$  (Figure 4.10c, where the relevant region is shaded), and hence complexifies the application of equations 4.18-4.19 for  $B$  to this case. Furthermore, many of the events that cross the VS patch occur right after other attempts, benefiting from elevated slip rate and stress on the VS patch from the previous attempt (as in Figure —4.10c), which significantly affects the slip rate  $V_{vs}^i$  in equation 4.19. However, the expression for the parameter  $B$  is still helpful in understanding why the QD simulations in the models with enhanced weakening are more likely to result in rupture propagation over the VS patch than the FD simulations. This is because the largest events that attempt to propagate over the patch have much larger values of  $\Delta\tau_{vw}$  in the QD simulations than in the FD simulations, up to a factor of 8 in the case considered in section 4.4.

Overall, the ability of the rupture to propagate over the VS patch is significantly affected by the FD vs. QD simulations in the models with enhanced dynamic weakening, as expected based on the significant differences between the simulations documented in section 4.4. Furthermore, the effect is not intuitive. One might intuitively think that the FD ruptures would be more likely to propagate through the patch, as observed in the cases with the standard rate-and-state friction, but this is not true in these models, since the QD simulations result in artificially large crack-like ruptures with much larger slip and stress drops, and hence have a significant edge in terms of their ability to propagate through the patch.

## 4.7 Conclusions

We have investigated the differences between the fully-dynamic (FD) simulations that properly incorporate the wave-mediated stress transfers and the quasi-dynamic (QD) simulations that ignore the transient nature of the stress transfers. The results support our hypothesis that the QD simulations can only be qualitatively useful in situations where the wave-mediated stress transfers do not produce important features that define the model response.

In the models with the standard rate-and-state friction and relatively uniform fault properties (section 4.3), the FD and QD simulations indeed produce qualitatively similar fault behaviors, with crack-like ruptures and similar earthquake patterns. There are also quantitative differences, with the FD simulations having fractionally larger amounts of slip per event, correspondingly larger stress drops, and significantly higher slip velocities and rupture speeds. These findings are similar to those of previous studies with similar models (*Lapusta et al.*, 2000; *Lapusta and Liu*, 2009). In terms of the ability of the rupture to propagate over the unfavorable spots such as the VS patch considered in this study, the trends with respect to the patch parameters are similar in the FD and QD simulations, but the events in the FD simulations are more likely to propagate over the patch for most cases considered, consistently with their higher stress drops, which is an important parameter, based on the study of *Kaneko et al.* (2010), and their higher slip rates and hence stress concentration.

However, the results of the FD and QD simulations become qualitatively different for the models with enhanced dynamic weakening, where we expect the wave-mediated stress changes to contribute to the formation of self-healing slip pulses (*Zheng and Rice*, 1998). Indeed, we find the FD simulations produce similar pulse-like ruptures that nucleate at the provided weaker site, whereas the QD simulations produce numerous smaller events at the edges of the seismogenic part of the model, until a much larger crack-like event spans the entire seismogenic part of the fault. The largest events in the QD simulations have much larger average slip and stress drop than the largest FD events, up to a factor of 8 in the cases considered. This finding is a clear reversal of what is observed in models with the standard rate-and-state friction, where the FD events are larger in slip and stress drop. Similarly to the models with the standard rate-and-state friction, the slip rate and rupture speed is significantly higher in the FD simulations with enhanced coseismic weakening than in the QD ones. However, unlike in the models with the standard rate-and-state friction, where the coseismic fault resistance is minimally affected, the higher slip rates in the models with enhanced coseismic weakening result in more pronounced fault weakening, and hence substantially change the fault behavior. In part, the average shear stress on the fault is significantly lower in the FD simulations, including before the largest model-spanning events, leading to self-healing pulse-like ruptures (*Zheng and Rice*, 1998; *Noda et al.*, 2009). As a result of their much larger slip and stress drop, the large events in the QD simulations are more likely to propagate through the unfavorable fault patch, again, contrary to the models with the standard rate-and-state friction. Note that the inability of the QD simulations to produce large sustained pulse-like events is particularly troubling in the view of observations that such mode of rupture propagation may be the one that operates on most mature faults (e.g., *Heaton*, 1990).

We expect similarly dramatic differences between the FD and QD simulations in other cases where wave-mediated transient effects can lead to qualitative differences. One of such cases is the models with transitions to supershear speeds (e.g., *Andrews*, 1976; *Xia et al.*, 2004; *Liu and Lapusta*,

2008), in which the wave-mediated stress transfers either produce a secondary supershear rupture ahead of the main one or induce the main rupture front to jump to the supershear speeds (*Liu and Lapusta, 2008*). Another case is that of strong local heterogeneities that can produce local arrest waves and cause short local rise time (e.g., *Beroza and Mikumo, 1996*), a phenomenon that may not be captured by the QD simulations.

Considering both models, we find that ignoring the transient wave-mediated stress transfers, which are a significant part of inertial effects, may lead to (1) mis-prediction of the size and recurrence of earthquakes; (2) incorrect average stress levels on the fault, and (3) missed characteristic features such as the sustained pulse-like mode of rupture propagation. Note that even the postseismic slip may be significantly affected, due to the differences in the coseismic rupture and its interaction with the potentially creeping VS fault areas.

We conclude that, to interpret correctly observations of individual earthquakes and the entire fault slip cycle, or to draw inferences regarding fault friction, it is important to use the right modeling approach. Under certain conditions, such as the standard rate-and-state friction and relatively homogeneous faults with no possibility of supershear transition, the QD simulations could be appropriate. However, since it is difficult to predict the outcome of the FD simulations and hence the presence or absence of certain features, it is important to verify the results with the FD approach at least for some representative cases.